ACS APPLIED MATERIALS & INTERFACES

www.acsami.org

Research Article

Structural Study of Polyacrylonitrile-Based Carbon Nanofibers for Understanding Gas Adsorption

Junbeom Park,* Ansgar Kretzschmar, Victor Selmert, Osmane Camara, Hans Kungl, Hermann Tempel, Shibabrata Basak,* and Rüdiger A. Eichel

Cite This: *ACS Appl. Mater. Interfaces* 2021, 13, 46665−46670

Read Online

ACCESS | Metrics & More | Article Recommendations | Supporting Information

ABSTRACT: Polyacrylonitrile-based carbon nanofibers (PAN-based CNFs) have great potential to be used for carbon dioxide (CO_2) capture due to their excellent CO_2 adsorption properties. The porous structure of PAN-based CNFs originates from their turbostratic structure, which is composed of numerous disordered stacks of graphitic layers. During the carbonization process, the internal structure is arranged toward the ordered graphitic structure, which significantly influences the gas adsorption properties of PAN-based CNFs. However, the relation between structural transformation and CO_2 capture is still not clear enough to tune the PAN-based CNFs. In this paper, we show that, with increasing carbonization temperature, the arrangement of the PAN-based CNF's structure along the stack and lateral directions takes place independently: gradually aligning and merging along the stack direction and enlarging along the lateral direction. Further, we correlate the structural arrangement and the CO_2 adsorption properties of the PAN-based CNFs to propose a comprehensive structural mechanism. This mechanism provides the knowledge to understand and tailor the gas adsorption properties of PAN-based CNFs.

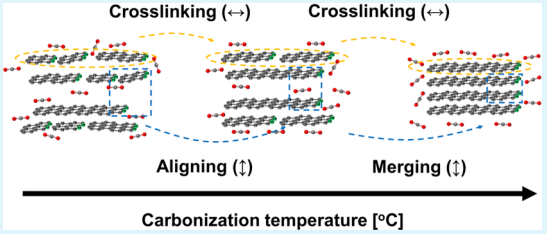

KEYWORDS: *PAN-based CNF, structural transformation, carbonization temperature, CO_2 adsorption, TEM, electron diffraction*

INTRODUCTION

Carbon capture and utilization not only can reduce the atmospheric carbon dioxide (CO_2) level but can also help to chemically transform CO_2 into value-added compounds as well, thus attracting much attention in recent years.[1,2] Conventionally, scrubbing through the amine solution has been used for CO_2 capture by chemical adsorption, but potentially harmful degradation products of amines and a considerable amount of energy demand for regeneration remain an issue.[3,4] Alternatively, studies have been made of physical adsorption-based CO_2 capture using microporous materials such as metal oxides (0.2−5.05 mmol/g at RT, 1 bar) or metal−organic frameworks (0.8−5.17 mmol/g at RT, 1 bar) and carbon-based materials (0.4−5.8 mmol/g at RT, 1 bar) have been studied.[5] Among them, metal oxides and metal−organic frameworks are comparatively sensitive toward water and may require harsh regeneration conditions.[4,6] In comparison, carbon-based materials are robust, environmentally friendly, and low cost, but the low selectivity remains a challenge. Polyacrylonitrile-based carbon nanofibers (PAN-based CNFs) offer a good adsorption capacity and a high selectivity even at lower pressure and are easy to fabricate toward commercial products.[7] Due to these reasons, PAN-based CNFs are considered as a promising material for CO_2 capture.

In general, optimization of the CO_2 adsorption capacity, specifically in PAN-based CNFs, involves enlarging the surface area or introducing the nitrogen functional groups.[8] In addition, the presence of ultramicropores can significantly enhance the adsorption of CO_2.[9] In the literature, various post-treated PAN-based CNFs are studied for their CO_2 adsorption properties.[10,11] However, less information is available on the CO_2 adsorption on unmodified PAN-based CNFs.

One work, investigating unmodified PAN-based CNFs, reported excellent CO_2 adsorption capacity on those carbonized at 800 °C or below.[12] However, the CO_2 adsorption capacity decreases significantly at carbonization temperatures from 800 to 1000 °C by more than a factor of 10 (Figure S1).[12] Accordingly, the number of accessible ultramicropores (<0.4 nm), which is critical to the CO_2 adsorption on these PAN-based CNFs, decreased as well.[9,12] This significant reduction of accessible ultramicropores was attributed to a shrinkage of the pore width with increasing carbonization temperature. Therefore, to optimize the PAN-based CNFs for CO_2 adsorption, a detailed understanding of the structural transformation mechanism during carbonization is essential. Fabrication of PAN-based CNFs is carried out by

Received: July 17, 2021
Published: September 21, 2021

https://doi.org/10.1021/acsami.1c13541
ACS Appl. Mater. Interfaces 2021, 13, 46665−46670

spinning, stabilization, and carbonization processes.[13−15] First, the electrospinning process, usually performed at room temperature, forms the primary polyacrylonitrile fiber. Then, during the stabilization process (<300 °C), a randomly stacked narrow ribbon-like structure is formed by cyclization. Finally, the carbonization process (>400 °C) converts and arranges toward the graphitic structure. Since the graphitic structures initially form at around 400−500 °C and become more crystalline and ordered at a higher carbonization temperature,[16,17] the electrical conductivity increases exponentially after 800 °C.[18]

Most of the reports on structural mechanisms of PAN-based CNFs only address carbonization temperatures above 1000 °C as these studies intend to obtain the thermodynamically preferable graphitic structure for mechanical applications.[19−21] However, these high carbonization temperatures are not favorable for CO_2 adsorption as this results in a significant reduction of the CO_2 adsorption capacity. Previously, Schierholz et al. reported on the structural change of PAN-based CNFs carbonized at intermediate temperatures (250−1000 °C), such as diameter, surface morphology, and alignment, via in situ TEM where the carbonization was performed in vacuum.[16] However, as the pressure during the carbonization may affect the structure of PAN-based CNFs,[22] a structural study of PAN-based CNFs prepared at ambient pressure is required to understand CO_2 adsorption on these PAN-based CNFs better.

According to the literature, the chemical transformation from the polymeric polyacrylonitrile to the graphitic structure proceeds via removing functional groups between 200 and 1400 °C.[18,23,24] Since the carbonization process combines both a physical and a chemical transformation, the correlation between these phenomena is required to understand the structural transformation mechanism and finally tune the ultramicropores of PAN-based CNFs for maximizing CO_2 adsorption. In this work, we investigate the structural changes of PAN-based CNFs carbonized at various temperatures by analyzing selected area electron diffraction (SAED) patterns of these PAN-based CNFs. With this technique, we analyze the structure of graphite-like crystallites in the PAN-based CNFs along the stack and lateral direction of graphitic layers. Furthermore, based on the results, a structural transformation mechanism is developed and helps to understand the CO_2 adsorption mechanism on PAN-based CNFs.

RESULTS AND DISCUSSION

To shed light on the structural transformation of PAN-based CNFs during the carbonization process, the structure of these PAN-based CNFs carbonized at various carbonization temperatures (600, 700, 800, 900, 1000, and 1100 °C) is studied via SAED. Figure 1a compares the SAED of PAN-based CNFs carbonized at 600 and 1100 °C. The SAEDs of all samples are given in Figure S2, Supporting Information, and representative TEM images are given in Figure S3. In all SAEDs, three ring patterns can be recognized, and as the temperature increases, these rings transform from diffused to sharp. The SAEDs of the PAN-based CNFs carbonized at 600 °C show blurry and diffuse rings, whereas the SAEDs of the PAN-based CNFs carbonized at 1100 °C show relatively clear and sharp rings (Figure 1a).

Figure 1b compares the SAED of PAN-based CNFs carbonized at 1100 °C with the theoretical SAED of graphite obtained using Difftools.[25] Figure 1c shows the (002) planes as well as the (10) and (11) lines of the graphitic structure. Compared with the theoretical SAED of graphite in Figure 1b, the first ring (the most inner ring) can be assigned to the (002) planes. However, a clear assignment of the second and third rings is not possible as these rings overlap with various planes: (100), (101), (102), and (004) for the second ring and (110), (112), and (006) for the third ring. Nonetheless, since carbonization temperatures are below 1100 °C, our PAN-based CNFs have a turbostratic structure, which is composed of randomly translated, rotated, or curved graphitic layers.[26] Generally, unlike graphite that is composed of ordered graphitic layers, the turbostratic structure is mainly described as the stack direction by (00*l*) planes and the lateral direction by (*hk*) lines.[27,28] Two-dimensional notation as (*hk*) lines can emphasize the transformation of individual graphitic layers rather than considering three-dimensional planes such as (101) planes that may not exist in the turbostratic structure. Thus, the three ring patterns in the SAED of the PAN-based CNFs can be assigned to the (002) planes, the (10) lines, and the (11) lines.

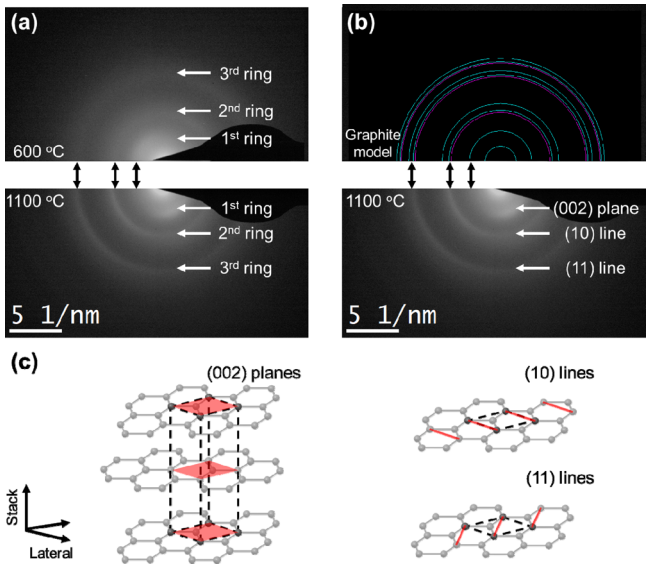

Figure 1. Comparison of selected area electron diffractions (SAEDs) of PAN-based CNFs carbonized at 1100 °C with (a) the SAED of PAN-based CNFs carbonized at 600 °C and (b) the SAED of graphite obtained using Difftools.[25] (c) Crystalline structure of graphite showing the (002) planes, (10) lines, and (11) lines.

Structural Change along the Stack Direction. To extract the structural details of the PAN-based CNFs from the SAEDs, first, all SAEDs are converted to intensity-radius spectra (Figure 2a-1 and Figure S4a). Second, peaks are selected from the converted spectra. Finally, the peak position and full width at half-maximum (FWHM) are obtained. Additionally, the first ring pattern has an angular intensity variation, which is also pronounced at higher carbonization temperatures (Figure S2). Therefore, intensity-angle spectra are extracted from the first ring of the SAEDs as well to obtain $FWHM_{angular}$ (Figure 2a-2 and Figure S4b). From the FWHM of the (002) planes and the (10) lines, the average height and width of the crystallites are calculated using the Bragg and Scherrer equations[21,29] (Figure S5).

In Figure 2b−d, the measured structural data (peak position, FWHM, and $FWHM_{angular}$) of the first ring patterns for PAN-based CNFs carbonized at various temperatures are plotted.

https://doi.org/10.1021/acsami.1c13541
ACS Appl. Mater. Interfaces 2021, 13, 46665−46670

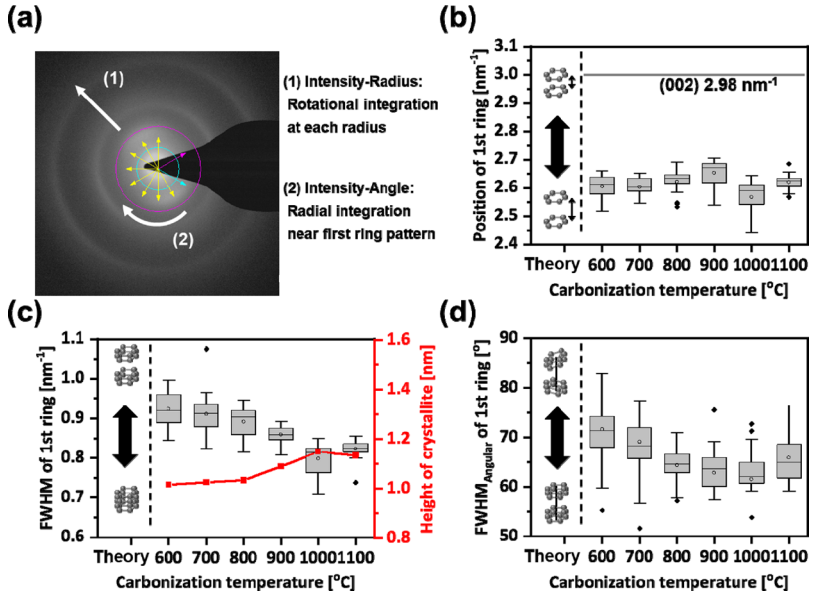

Figure 2. (a) Scheme of the integration of a SAED pattern into the spectra. Box plots of the (b) peak position, (c) FWHM, and (d) FWHM$_{angular}$ of the first ring pattern in the SAED patterns of PAN-based CNFs carbonized at various temperatures.

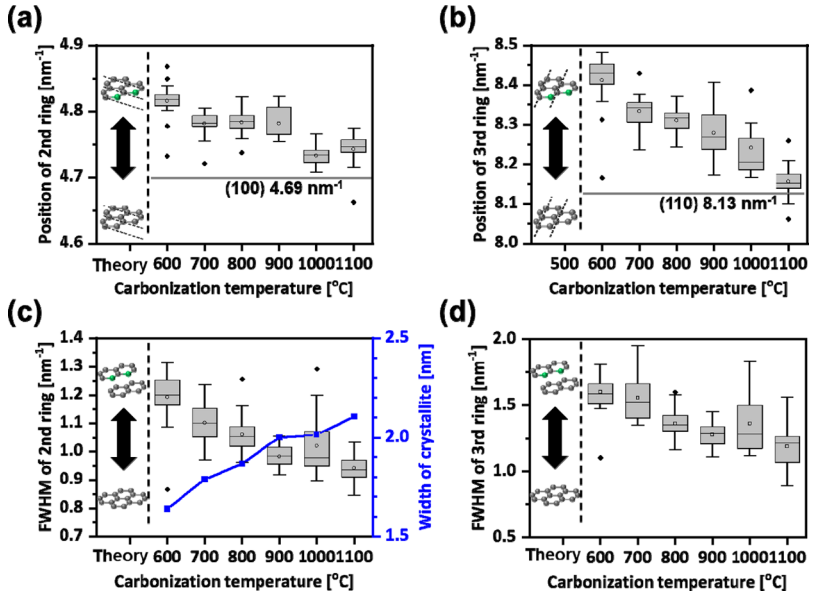

Figure 3. Box plots of the peak position (a, b) and FWHM (c, d) of the second and third ring patterns in the SAED patterns of PAN-based CNFs carbonized at various temperatures.

All the peak positions of the first ring are constant around 2.6 nm^{-1} and clearly lower than the value of graphite (2.98 nm^{-1}) (Figure 2b). According to the Bragg equation, the lower position indicates a larger distance between representing crystal planes. For the (002) planes of PAN-based CNFs, the distance between graphitic layers is larger than graphite. This is a reasonable result as the commercial graphitization process treats the carbon at 1500−3000 °C.[14] However, the carbonization temperature used in this paper is significantly lower (600−1100 °C), leading to less densely stacked graphite-like layers. The previous studies also proved from X-ray diffraction data that the peak position of the (002) plane of the PAN-based CNFs carbonized at 400−1300 °C did not show a significant shift.[17,29,30]

The FWHM of the first ring decreases significantly from the PAN-based CNFs carbonized at 800 °C to the PAN-based CNFs carbonized at 1000 °C (Figure 2c). Referring to the Scherrer equation, the decrease in FWHM indicates that the crystallite size along the stack direction (height of crystallite) increases. This increase from the merging process probably occurs by stacking with adjacent crystallites. The FWHM$_{angular}$ of the first ring decreases from PAN-based CNFs carbonized at 600 °C to PAN-based CNFs carbonized at 800 °C and then stabilizes (Figure 2d). The decrease in FWHM$_{angular}$ indicates that the crystallites are more aligned parallel to the surface.[16] From the above result, the structure arrangement along the stack direction can be described in two steps: first, aligning parallel to the surface from carbonization temperatures of

https://doi.org/10.1021/acsami.1c13541
ACS Appl. Mater. Interfaces 2021, 13, 46665−46670

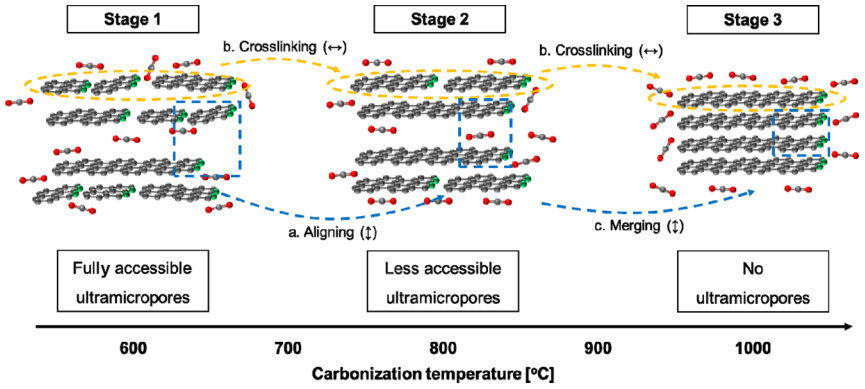

Figure 4. Schematic representation of the proposed structural transformation mechanism during the carbonization process. Green atoms indicate the heteroatoms in the PAN-based CNFs.

600−800 °C and, second, merging from carbonization temperatures of 800−1000 °C.

Structural Change along the Lateral Direction. In Figure 3, the measured structural data of the second and third ring patterns for PAN-based CNFs carbonized at various temperatures are plotted. With increasing carbonization temperature, the peak position of the second ring moves stepwise inward (Figure 3a), while the position of the third ring moves gradually inward (Figure 3b). However, both the peak positions of the second ring and the peak position of the third ring approach the corresponding value of graphite. Similar to the first ring, the lower peak position indicates a larger distance between representing crystal planes. For both the (10) lines and (11) lines of PAN-based CNFs, the size of the six-membered ring increases toward graphite. Kretzschmar et al. reported that PAN-based CNFs carbonized at 600 °C contained 20 at % of nitrogen and 4 at % of oxygen and that the contents of PAN-based CNFs carbonized at 1100 °C reduce to 3 and 2 at %, respectively.[12] Since the C═O and C═N bonds are 0.06−0.1 Å shorter than the C═C bonds,[31] the inward movement of the second and third ring can be caused by removing heteroatoms in the PAN-based CNFs.

The FWHM of the second and third rings decreases gradually up to a carbonization temperature of 1100 °C (Figure 3c,d). As for the first ring, the decrease in the FWHM indicates that the crystallite size increases. In contrast to the first ring, the crystallite growth proceeds along the lateral direction (width of the graphitic layer). The layer enlargement of the PAN-based CNFs is attributed to cross-linking of adjacent layers by the removal of heteroatoms.[15] Similar to the discussion about the peak position above, the removal of oxygen and nitrogen takes place. According to the literature, oxygen is removed as H_2O, CO, or CO_2, and nitrogen is removed as NH_3, HCN, or N_2 with cross-linking reaction between graphitic layers from PAN-based CNFs during the carbonization process.[15,32] The enlargement of the graphitic layers can directly enhance the conductivity,[18] making the carbonization temperature important to tailor the electrical properties of these PAN-based CNFs.

Structural Transformation Mechanism in Correlation to the CO_2 Adsorption. Based on the above discussions, we propose a comprehensive structural change mechanism of PAN-based CNFs during the carbonization process described schematically in Figure 4. Along the stack direction, crystallites are aligned parallel to the fiber surface up to a carbonization temperature of 800 °C and then merged into thicker crystallites by stacking up to a carbonization temperature of 1000 °C. Along the lateral direction, the graphitic layers are enlarged continuously by cross-linking with adjacent layers up to a carbonization temperature of 1100 °C. The cross-linking reaction takes place by the removal of heteroatoms.

From a previous study, the adsorption capacity of CO_2 in PAN-based CNFs vastly decreased at the carbonization temperature range from 800 to 1000 °C (Figure S1).[12] In PAN-based CNFs, CO_2 molecules have three possible adsorption places: first in the gap between graphitic layers like Li intercalation into graphite in secondary batteries,[33] second at the edge of graphitic layers, or last on the surface of crystallites. From our experiments, the distance between the graphitic layers of PAN-based CNFs is constant throughout different carbonization temperatures (Figure 2b). Furthermore, the amount of layer edges decreases continuously over the whole range of the studied carbonization temperatures as the layers are enlarged by cross-linking (Figure 3c). On the other hand, the amount of crystallite surface decreased primarily between 800 and 1000 °C as the crystallites merged (Figure 2c). Thus, based on SAED analysis, we assume that the majority of CO_2 adsorption takes place on the crystallite surface and between the crystallites, which forms the ultramicropores. Whether the CO_2 adsorption on the crystallite surface occurs majorly near the surface of the PAN-based CNFs or uniformly throughout the CNFs is subject to further studies.

■ CONCLUSIONS

Based on the structural details of PAN-based CNFs analyzed with SAEDs, we developed a comprehensive structural transformation mechanism of PAN-based CNFs during the carbonization process. This model successfully explains the change of CO_2 adsorption properties of PAN-based CNFs during the carbonization process: The gap between graphitic layers in the crystallite stays far wider than in graphite during the whole carbonization temperature range. Along the stack direction, the crystallites are aligned parallel up to a carbonization temperature of 800 °C and then are merged into thicker crystallites by stacking up to a carbonization temperature of 1000 °C. Along the lateral direction, the graphitic layers are enlarged by cross-linking up to a carbonization temperature of 1100 °C. By correlating the structural transformation mechanism and gas adsorption studies, we speculate that merging crystallites along the stack direction is the main factor affecting the CO_2 adsorption

https://doi.org/10.1021/acsami.1c13541
ACS Appl. Mater. Interfaces 2021, 13, 46665−46670

capacity. The developed mechanism can help to tailor the PAN-based CNFs to the desired gas adsorption properties.

EXPERIMENTAL SECTION

Fabrication of PAN-Based CNFs by Electrospinning.[12] PAN-based CNFs were fabricated by the electrospinning method and subsequent heat treatments. Briefly, a solution containing 10 wt % PAN (150,000 g/mol, BOC Science, USA) in DMF (VWR Chemicals, Germany) was electrospun (25 kV, 15 cm distance, 40 μL/min, 25 °C, 30% relative humidity) and PAN nanofibers were collected. The obtained nanofibers were dried in air for 1 h at 150 °C and then stabilized in air for 15 h at 250 °C. Finally, the stabilized nanofibers were carbonized in argon for 3 h at constant temperatures (600, 700, 800, 900, 1000, and 1100 °C).

Characterization and Analysis. From each sample carbonized at various temperatures, SAEDs from 20 different fibers and TEM images were obtained and analyzed (Figure 1 and Figure S2-3). The SAEDs and TEM images of the PAN-based CNFs were analyzed by transmission electron microscopy (TEM; Tecnai, Thermo Fisher Scientific) at 200 kV with a 300 mm camera length.

The obtained SAEDs were converted to background-subtracted intensity-radius spectra by rotational integration at each radius (Figure 2a-1 and Figure S4a) using the Difftools plugin in DigitalMicrograph.[25] The spectra were fitted by OriginPro to obtain the peak position and full width at half-maximum (FWHM). The crystallite size was calculated from FWHM by using Bragg and Scherrer equations (Figure S5).[21,29] Additionally, the background-subtracted intensity-angle spectra (Figure 2a-2 and Figure S4b) were prepared by radial integration at each angle near the first ring using the Difftools plugin at DigitalMicrograph.[25] The spectra were fitted by OriginPro to obtain the $FWHM_{angular}$. Each obtained data point (peak position, FWHM, and $FWHM_{angular}$) was drawn as a box plot, showing the distribution of the data statistically (Figure S6).

ASSOCIATED CONTENT

Supporting Information

The Supporting Information is available free of charge at https://pubs.acs.org/doi/10.1021/acsami.1c13541.

> Gas adsorption, pore volume, SAED patterns, TEM images and obtained spectra of PAN-based CNFs carbonized at various temperatures, and the description of data converting and box plot (PDF)

AUTHOR INFORMATION

Corresponding Authors

Junbeom Park − *Institute of Energy and Climate Research - Fundamental Electrochemistry (IEK-9), Forschungszentrum Jülich GmbH, 52425 Jülich, Germany; Institute of Inorganic Chemistry, RWTH Aachen University, 52074 Aachen, Germany;* orcid.org/0000-0003-2548-2985; Email: j.park@fz-juelich.de

Shibabrata Basak − *Institute of Energy and Climate Research - Fundamental Electrochemistry (IEK-9) and Ernst Ruska-Centre for Microscopy and Spectroscopy with Electrons, Forschungszentrum Jülich GmbH, 52425 Jülich, Germany;* orcid.org/0000-0002-4331-4742; Email: s.basak@fz-juelich.de

Authors

Ansgar Kretzschmar − *Institute of Energy and Climate Research - Fundamental Electrochemistry (IEK-9), Forschungszentrum Jülich GmbH, 52425 Jülich, Germany; Institute of Physical Chemistry, RWTH Aachen University, 52074 Aachen, Germany*

Victor Selmert − *Institute of Energy and Climate Research - Fundamental Electrochemistry (IEK-9), Forschungszentrum Jülich GmbH, 52425 Jülich, Germany; Institute of Physical Chemistry, RWTH Aachen University, 52074 Aachen, Germany;* orcid.org/0000-0002-1196-2542

Osmane Camara − *Institute of Energy and Climate Research - Fundamental Electrochemistry (IEK-9), Forschungszentrum Jülich GmbH, 52425 Jülich, Germany*

Hans Kungl − *Institute of Energy and Climate Research - Fundamental Electrochemistry (IEK-9), Forschungszentrum Jülich GmbH, 52425 Jülich, Germany*

Hermann Tempel − *Institute of Energy and Climate Research - Fundamental Electrochemistry (IEK-9), Forschungszentrum Jülich GmbH, 52425 Jülich, Germany;* orcid.org/0000-0002-9794-6403

Rüdiger A. Eichel − *Institute of Energy and Climate Research - Fundamental Electrochemistry (IEK-9), Forschungszentrum Jülich GmbH, 52425 Jülich, Germany; Institute of Physical Chemistry, RWTH Aachen University, 52074 Aachen, Germany;* orcid.org/0000-0002-0013-6325

Complete contact information is available at: https://pubs.acs.org/10.1021/acsami.1c13541

Notes

The authors declare no competing financial interest.

ACKNOWLEDGMENTS

The authors, J.P., H.T., H.K., and O.C., acknowledge funding provided by the Bundesministerium für Bildung und Forschung, the project iNEW FKZ 03F0589A (BMBF, German Research Foundation). V.S. acknowledges funding provided by the Deutsche Forschungsgemeinschaft (DFG, German Research Foundation) under Germany's Excellence Strategy − Cluster of Excellence 2186 "The Fuel Science Center" − ID: 390919832. S.B. acknowledges "Electroscopy" (grant no. 892916) from the Marie Sklodowska-Curie action.

REFERENCES

(1) Keller, L.; Ohs, B.; Lenhart, J.; Abduly, L.; Blanke, P.; Wessling, M. High Capacity Polyethylenimine Impregnated Microtubes Made of Carbon Nanotubes for CO_2 Capture. *Carbon* **2018**, *126*, 338−345.

(2) Foit, S. R.; Vinke, I. C.; de Haart, L. G. J.; Eichel, R.-A. Power-to-Syngas: An Enabling Technology for the Transition of the Energy System? *Angew. Chem., Int. Ed.* **2017**, *56*, 5402−5411.

(3) Dutcher, B.; Fan, M.; Russell, A. G. Amine-Based CO_2 Capture Technology Development from the Beginning of 2013—A Review. *ACS Appl. Mater. Interfaces* **2015**, *7*, 2137−2148.

(4) D'Alessandro, D. M.; Smit, B.; Long, J. R. Carbon Dioxide Capture: Prospects for New Materials. *Angew. Chem., Int. Ed.* **2010**, *49*, 6058−6082.

(5) Pardakhti, M.; Jafari, T.; Tobin, Z.; Dutta, B.; Moharreri, E.; Shemshaki, N. S.; Suib, S.; Srivastava, R. Trends in Solid Adsorbent Materials Development for CO_2 Capture. *ACS Appl. Mater. Interfaces* **2019**, *11*, 34533−34559.

(6) Spigarelli, B. P.; Kawatra, S. K. Opportunities and Challenges in Carbon Dioxide Capture. *J. CO2 Util.* **2013**, *1*, 69−87.

(7) Yamamoto, T.; Tryk, D. A.; Hashimoto, K.; Fujishima, A.; Okawa, M. Electrochemical Reduction of CO_2 in the Micropores of Activated Carbon Fibers. *J. Electrochem. Soc.* **2000**, *147*, 3393−3400.

(8) Sethia, G.; Sayari, A. Comprehensive Study of Ultra-Microporous Nitrogen-Doped Activated Carbon for CO_2 Capture. *Carbon* **2015**, *93*, 68−80.

(9) Zhang, Z.; Zhou, J.; Xing, W.; Xue, Q.; Yan, Z.; Zhuo, S.; Qiao, S. Z. Critical Role of Small Micropores in High CO_2 Uptake. *Phys. Chem. Chem. Phys.* **2013**, *15*, 2523−2529.

(10) Shen, W.; Zhang, S.; He, Y.; Li, J.; Fan, W. Hierarchical Porous Polyacrylonitrile-Based Activated Carbon Fibers for CO_2 Capture. *J. Mater. Chem.* **2011**, *21*, 14036−14040.
(11) Li, L.; Wang, X.-F.; Zhong, J.-J.; Qian, X.; Song, S.-L.; Zhang, Y.-G.; Li, D.-H. Nitrogen-Enriched Porous Polyacrylonitrile-Based Carbon Fibers for CO_2 Capture. *Ind. Eng. Chem. Res.* **2018**, *57*, 11608−11616.
(12) Kretzschmar, A.; Selmert, V.; Weinrich, H.; Kungl, H.; Tempel, H.; Eichel, R. Tailored Gas Adsorption Properties of Electrospun Carbon Nanofibers for Gas Separation and Storage. *ChemSusChem* **2020**, *13*, 3180−3191.
(13) Frank, E.; Hermanutz, F.; Buchmeiser, M. R. Carbon Fibers: Precursors, Manufacturing, and Properties. *Macromol. Mater. Eng.* **2012**, *297*, 493−501.
(14) Park, S.-J. *Carbon Fibers*; Springer Series in Materials Science. Springer Singapore: Singapore 2018, *210*, DOI: 10.1007/978-981-13-0538-2.
(15) Rahaman, M. S. A.; Ismail, A. F.; Mustafa, A. A Review of Heat Treatment on Polyacrylonitrile Fiber. *Polym. Degrad. Stab.* **2007**, *92*, 1421−1432.
(16) Schierholz, R.; Kröger, D.; Weinrich, H.; Gehring, M.; Tempel, H.; Kungl, H.; Mayer, J.; Eichel, R.-A. The Carbonization of Polyacrylonitrile-Derived Electrospun Carbon Nanofibers Studied by *in Situ* Transmission Electron Microscopy. *RSC Adv.* **2019**, *9*, 6267−6277.
(17) Lee, S.; Kim, J.; Ku, B.-C.; Kim, J.; Joh, H.-I. Structural Evolution of Polyacrylonitrile Fibers in Stabilization and Carbonization. *Adv. Chem. Eng. Sci.* **2012**, *02*, 275−282.
(18) Gehring, M.; Tempel, H.; Merlen, A.; Schierholz, R.; Eichel, R.-A.; Kungl, H. Carbonisation Temperature Dependence of Electrochemical Activity of Nitrogen-Doped Carbon Fibres from Electrospinning as Air-Cathodes for Aqueous-Alkaline Metal-Air Batteries. *RSC Adv.* **2019**, *9*, 27231−27241.
(19) Liu, F.; Wang, H.; Xue, L.; Fan, L.; Zhu, Z. Effect of Microstructure on the Mechanical Properties of PAN-Based Carbon Fibers during High-Temperature Graphitization. *J. Mater. Sci.* **2008**, *43*, 4316−4322.
(20) Musiol, P.; Szatkowski, P.; Gubernat, M.; Weselucha-Birczynska, A.; Blazewicz, S. Comparative Study of the Structure and Microstructure of PAN-Based Nano- and Micro-Carbon Fibers. *Ceram. Int.* **2016**, *42*, 11603−11610.
(21) Ko, T. Raman Spectrum of Modified PAN-based Carbon Fibers during Graphitization. *J. Appl. Polym. Sci.* **1996**, *59*, 577.
(22) Song, C.; Wang, T.; Qiu, Y.; Qiu, J.; Cheng, H. Effect of Carbonization Atmosphere on the Structure Changes of PAN Carbon Membranes. *J. Porous Mater.* **2009**, *16*, 197−203.
(23) Laffont, L.; Monthioux, M.; Serin, V.; Mathur, R. B.; Guimon, C.; Guimon, M. F. An EELS Study of the Structural and Chemical Transformation of PAN Polymer to Solid Carbon. *Carbon* **2004**, *42*, 2485−2494.
(24) Bromley, J. Gas Evolution Processes during the Formation of Carbon Fibres. In *International conference on Carbon Fibres, their Composites and Applications*; World Academy of Science, Engineering and Technology: 1971; p Paper No. 1.
(25) Mitchell, D. R.; DiffTools, G. Electron Diffraction Software Tools for DigitalMicrograph™. *Microsc. Res. Tech.* **2008**, *71*, 588−593.
(26) Li, Z. Q.; Lu, C. J.; Xia, Z. P.; Zhou, Y.; Luo, Z. X-Ray Diffraction Patterns of Graphite and Turbostratic Carbon. *Carbon* **2007**, *45*, 1686−1695.
(27) Fujimoto, H. Theoretical X-Ray Scattering Intensity of Carbons with Turbostratic Stacking and AB Stacking Structures. *Carbon* **2003**, *41*, 1585−1592.
(28) Babu, V. S.; Seehra, M. S. Modeling of Disorder and X-Ray Diffraction in Coal-Based Graphitic Carbons. *Carbon* **1996**, *34*, 1259−1265.
(29) Kim, C.; Park, S.-H.; Cho, J.-I.; Lee, D.-Y.; Park, T.-J.; Lee, W.-J.; Yang, K.-S. Raman Spectroscopic Evaluation of Polyacrylonitrile-Based Carbon Nanofibers Prepared by Electrospinning. *J. Raman Spectrosc.* **2004**, *35*, 928−933.
(30) Zhu, C.-Z.; Yu, X.-L.; Liu, X.-F.; Mao, Y.-Z.; Liu, R.-G.; Zhao, N.; Zhang, X.-L.; Xu, J. 2D SAXS/WAXD Analysis of Pan Carbon Fiber Microstructure in Organic/Inorganic Transformation. *Chin. J. Polym. Sci.* **2013**, *31*, 823−832.
(31) Raczyńska, E. D.; Hallman, M.; Kolczyńska, K.; Stępniewski, T. M. On the Harmonic Oscillator Model of Electron Delocalization (HOMED) Index and Its Application to Heteroatomic π-Electron Systems. *Symmetry* **2010**, *2*, 1485−1509.
(32) Watt, W.; Green, J. The Pyrolysis of Polyacrylonitrile. In *International conference on Carbon Fibres, their Composites and Applications, London*; Plastics Institute: 1971; p Paper No. 4.
(33) Xu, J.; Dou, Y.; Wei, Z.; Ma, J.; Deng, Y.; Li, Y.; Liu, H.; Dou, S. Recent Progress in Graphite Intercalation Compounds for Rechargeable Metal (Li, Na, K, Al)-Ion Batteries. *Adv. Sci.* **2017**, *4*, 1700146.